The Effect Of Heat On The Diversion Length Of Capillary Barriers

[1] C.J. Matthews, [1]J.H. Knight, [2]F.J. Cook and [1]R.D. Braddock

[1]Griffith University, School of Environmental Engineering, Nathan, [2]CSIRO Land and Water, Indooroopilly, QLD E-Mail: c.matthews@griffith.edu.au .

Keywords: Capillary Barrier, heat, unsaturated flow, layered soils

EXTENDED ABSTRACT

Within the literature, capillary barriers have been suggested as an alternative hydraulic barrier in cover liners for waste dumps. When a waste dump reaches its full capacity, cover liners are usually constructed over the waste mound to seal the waste from the surrounding environment. One main function of a cover liner is to prevent substantial amounts of water infiltrating into the waste material thereby preventing leaching and potentially contamination of the ground water system. A capillary barrier consists of a fine soil overlying a coarse soil, which can impeded infiltrating water at the soil layer interface by capillary forces. Breakthrough into the coarse soil will only occur once enough water has accumulated at the interface to overcome the water-entry pressure of the coarse soil. If a capillary barrier is inclined, water will flow laterally downslope (or upslope) until breakthrough is reached. The length of this lateral flow, parallel to the slope, is known as the diversion length. Additionally, sealed waste can produce a substantial amount of heat due to the decomposing waste material. Therefore, it is important to explore the effect of heat on the performance of capillary barriers.

This paper will explore the effect of heat on the diversion length of a capillary barriers by using a numerical model based on the Method of Lines. The model will be used to simulate one-dimensional coupled heat and water flow through a capillary barrier consisting of a Glendale clay loam over Berino fine sand. The domain will be rotated by a given angle and will represent flow through an elongated slope where the edge effects can be ignored. It will be assumed that the underlying waste will generate a constant heat source while the soil surface experiences a constant water flux. Under these conditions, the heat generated by the waste will result in heat and water fluxes moving up the soil profile towards the soil surface opposing the infiltrating water flux. To estimate the divergence length of the capillary barrier, the analytical solution of Warrick et al (1997) for divergence length of isothermal steady-state flow through layered soils will be extended to non-isothermal conditions. This does not provide an absolute analytical solution for divergence length under non-isothermal conditions since the solution still requires information from the steady-state numerical solution.

It will be shown that heat generated from the waste will have a dramatic effect on the divergence length of the capillary barrier when compared to the isothermal case. In particular, under dry conditions, the heat processes will dominate resulting in upslope divergence. Under the same water flow conditions, downslope divergence is expected for isothermal flow. Interestingly, as the surface flux is increased, the results show that, for non-isothermal flow, the divergence length switches from an upslope divergence to a downslope divergence. This is the direct opposite to isothermal flow where downslope eventual occurs as the surface flux is increased. Essentially, heat seems to act as an additional barrier to promote flow down a slope and away from the underlying waste.

This result has implications for cover liner design since it appears to extend the use of capillary barriers for higher surface fluxes. However, given the dynamic nature of the heat fluxes from waste and the uncertainty in its behaviour, the non-isothermal flow of water through cover liner design will have to be explored in more detail.

1. INTRODUCTION

The majority of waste from society, whether it be municipal or mining, is disposed of in landfills. Fundamentally, the objective of a landfill is isolate potentially harmful waste from the surrounding environment until the waste decomposes to a less harmful state (Koerner and Daniel, 1997). Once a landfill reaches its design capacity, a cover liner is constructed over the waste as a seal to the environment. One of the most important functions of a cover liner is to minimise the amount of water that infiltrates into the waste material and, consequently, prevent excessive amounts of leachate entering the underlying groundwater system (Koerner and Daniel, 1997). The hydraulic barrier component of a cover liner system is generally engineered using compacted clays and/or geosynthetic materials due to their low saturated hydraulic conductivity properties. However, the longevity of these types of barriers is questionable. Geosynthetic materials can be damaged during construction resulting in weak zones or puncture holes that can cause preferential flow paths (Daniel, 1995). Similarly, compacted clays can crack from wetting and drying processes, particularly, when high temperature gradients are evident (Nassar et al, 1996).

Capillary barriers have been suggested as an alternative hydraulic barrier within cover liner systems. A capillary barrier consists of a fine soil overlying a coarse soil, which impedes the flow of infiltrating water at the interface due to the strong capillary forces of the fine soil (Warrick et al, 1997). Water will only move into the coarse soil once enough water as accumulated at the interface to exceed the air entry pressure of the coarse soil (Walter et al, 2000). If a capillary barrier is inclined, water will flow laterally down-slope (or up-slope) until breakthrough is reached. The length of this lateral flow, parallel to the slope, is known as the diversion length (Warrick et al, 1997).

Once sealed from the environment, the decomposing waste material in a landfill can generate large amounts of heat that can have a dramatic effect on water flow through layered soil profile. Recently, Nassar and Horton (1997) showed experimentally, and numerically, for a vertical soil profile that diurnal temperature effects of the surface caused greater thermal water transfer than isothermal water transfer in layered compacted soils. Other studies within the literature have also explored the combined effect of heat and water flow through compacted clay liners in landfills, which aimed to examine conditions that can lead to cracking of the compacted soil (Nassar et al, 1996). However, to date, the effect of heat on the divergence length of capillary barriers has not been investigated.

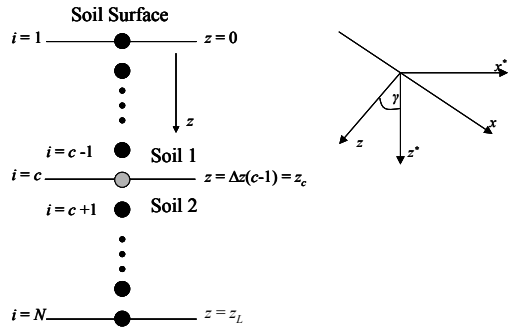

Figure 1 Layered soil profiles and grid system along the rotated coordinate system (z).

This study will model one-dimensional coupled heat and water flow through a capillary barrier for a rotated coordinate system given by Figure 1. The model will represent flow along an elongated slope where flow in the lateral direction (along the x-axis) can be neglected. The capillary barrier will consist of two soils: Glendale clay loam (Soil 1) over Berino fine sand (Soil 2), which will be inclined by an angle γ. The model will be used to explore the effect of infiltrating water from a constant surface flux as it meets a constant heat source from the bottom of the soil profile. In particular, we will show to what extent heat generated by the underlying waste can affect the diversion length of capillary barriers. This will be achieved by extending the analytical solution of Warrick et al (1997) for the diversion length of capillary barriers to the non-isothermal case.

2. GOVERNING EQUATIONS

2.1 Coupled Heat and Water flow.

The coupled heat and unsaturated water flow equations of Philip and de Vries (1957) can be expressed in rotated form (Figure 1) as

$$\frac{\partial \theta_k}{\partial t} = \frac{\partial}{\partial z}\left(D_{Tk} \frac{\partial T_k}{\partial z} \right) + \frac{\partial}{\partial z}\left(D_{\theta k} \frac{\partial \theta}{\partial z} \right) - \cos(\gamma) \frac{\partial K_{\theta l k}}{\partial z}, \quad (1)$$

$$C_{Tk} \frac{\partial T_k}{\partial t} = \frac{\partial}{\partial z}\left(\lambda_k \frac{\partial T_k}{\partial z} \right) + L \frac{\partial}{\partial z}\left(D_{Tvk} \frac{\partial T_k}{\partial z} + D_{\theta vk} \frac{\partial \theta_k}{\partial z} \right), \quad (2)$$

subject to the following initial and boundary conditions for water transfer

$$\left.\begin{aligned} \theta_i &= \theta_{i1}, \quad z \in [0, z_c] \\ \theta_i &= \theta_{i2}, \quad z \in [z_c, z_L] \end{aligned}\right\}, \quad t = 0, \quad (3)$$

$$\frac{\partial \theta_1}{\partial z} = \frac{(K(\theta_1) - q_s)\cos(\gamma)}{D(\theta_1)} - \frac{D_T(\theta_1, T_1)}{D(\theta_1)} \frac{\partial T}{\partial z} \quad z = 0, \quad t \geq 0, \quad (4)$$

$$\left.\begin{aligned} \psi_1(\theta_1) &= \psi_2(\theta_2) \\ q_{\theta 1}(\theta_1, T_1) &= q_{\theta 2}(\theta_2, T_2) \end{aligned}\right\}, \quad z = z_c, \quad t \geq 0, \quad (5)$$

$$\frac{\partial \theta_2}{\partial z} = 0, \quad z = z_L, \quad t \geq 0, \quad (6)$$

and heat transfer

$$T_i = 20°\text{C}, \quad z \in [0, z_L], \quad t = 0, \quad (7)$$

$$T = 20°\text{C}, \quad z = 0, \quad t \geq 0, \quad (8)$$

$$\left.\begin{aligned} T_1 &= T_2 \\ q_{h1}(T_1, \theta_1) &= q_{h2}(T_2, \theta_2) \end{aligned}\right\}, \quad z = z_c, \quad t \geq 0, \quad (9)$$

$$T_2 = 50°\text{C}, \quad z = z_L, \quad t \geq 0, \quad (10)$$

where $D_T = D_{Tl} + D_{Tv}$ is thermal moisture diffusivity ($\text{cm}^2\ \text{sec}^{-1}\ {}^{o}\text{C}^{-1}$), $D_\theta = D_{\theta l} + D_{\theta v}$ is the isothermal moisture diffusivity ($\text{cm}^2\ \text{sec}^{-1}$), D_{Tl} is the thermal liquid diffusivity ($\text{cm}^2\ \text{sec}^{-1}\ {}^{o}\text{C}^{-1}$), D_{Tv} is the thermal vapour diffusivity ($\text{cm}^2\ \text{sec}^{-1}\ {}^{o}\text{C}^{-1}$), λ is the thermal conductivity (cal $\text{cm}^{-1}\ \text{sec}^{-1}\ {}^{o}\text{C}^{-1}$), C_T is the volumetric heat capacity of the soil (cal $\text{cm}^{-3}\ {}^{o}\text{C}^{-1}$), q_v is the vapour flux (g $\text{cm}^{-2}\ \text{sec}^{-1}$), T is temperature (°C), L = 585 (cal/g) is latent heat of vaporisation, ψ is matric potential (cm), t is time (sec), z is a coordinate normal to the sloping surface positive downwards (cm) and subscript k (=1 or 2) denotes soil type as depicted in Figure 1. Equations (1) and (2) are based on the conservation of mass and energy with moisture and heat fluxes given by

$$q_{\theta k} = -D_{Tk} \frac{\partial T_k}{\partial z} - D_{\theta k} \frac{\partial \theta_k}{\partial z} + K_k \cos(\gamma), \quad (11)$$

and

$$q_h = -\lambda_k \frac{\partial T_k}{\partial z} - L\left(D_{Tvk} \frac{\partial T_k}{\partial z} + D_{\theta vk} \frac{\partial \theta_k}{\partial z} \right), \quad (12)$$

respectively. The constitutive equations are given by

$$D_{Tl} = K_{\theta l} \xi \psi, \quad (13)$$

$$D_{Tv} = \eta \alpha a D_a v \frac{d\rho_{vs}}{dT}, \quad (14)$$

$$D_{\theta v} = \frac{\alpha a D_a v g \rho_v}{\rho_l R T} \frac{d\psi}{d\theta}, \quad (15)$$

$$\lambda = \lambda_a + \lambda_v = \lambda_a + L D_a v h_r \frac{d\rho_{vs}}{dT}, \quad (16)$$

$$C = 0.48 X_m + 0.6 X_o + \theta, \quad (17)$$

where ξ = -2.09x10^{-3} is temperature coefficient of water surface tension ($^{o}\text{C}^{-1}$), η is the vapour flow enhancement factor, α = 2/3 is tortuosity factor, a = $S - \theta$ is the volumetric air content (cm^3/cm^3), S is porosity, D_a is the coefficient for molecular diffusion of water vapour in air ($\text{cm}^2\ \text{sec}^{-1}$), v is the mass flow factor, ρ_{vs} is density of saturated water vapour (g cm^{-3}), g is acceleration due to gravity (cm sec^{-1}), ρ_v is density of water vapour (g cm^{-3}), ρ_l is the density of liquid water (g cm^{-3}), R = 4.615x10^6 is the gas constant of water vapour (erg $\text{g}^{-1}\ {}^{o}\text{C}^{-1}$), λ_a = 5.82e-5 is the thermal conductivity of air (cal $\text{cm}^{-1}\ \text{sec}^{-1}\ {}^{o}\text{C}^{-1}$), h_r is relative humidity and X_m and X_o is the volume fraction of mineral and organic matter in the soil respectively. Note that $D_{\theta l}$, $K_{\theta l}$ and $d\theta/d\psi$ are the isothermal hydraulic diffusivity ($\text{cm}^2\ \text{s}^{-1}$), hydraulic conductivity ($\text{cm}\ \text{s}^{-1}$) and water capacity (cm^{-1}), respectively and are describe by the van Genuchten (1980) equations. In addition, temperature and water content dependent variables within (13)-(17) are calculated as per Philip and de Vries (1957) except for η, which is given by (Scanlon et al, 2003)

$$\eta = 9.5 + 3\frac{\theta}{\theta_s} - 8.5 \exp\left[-\left[\left(1 + \frac{2.6}{\sqrt{f_c}} \right) \frac{\theta}{\theta_s} \right]^4 \right], \quad (18)$$

where f_c is the mass fraction of clay in the soil.

2.2 Water flow in isothermal conditions.

One-dimensional unsaturated flow under isothermal conditions for the rotated coordinate system is given by Richards' Equation as

$$\frac{\partial \hat{\theta}}{\partial t} = \frac{\partial}{\partial z}\left(D_{\theta l} \frac{\partial \hat{\theta}}{\partial z} \right) - \cos(\gamma) \frac{\partial K_{\theta l}}{\partial z}, \quad (19)$$

where the ^ represents the solution of the isothermal case. (19) will be solved subject to the same type of initial and boundary conditions as expressed above for (1). Note that the isothermal water flux is given by

$$\hat{q}_w = -D_{\theta l} \frac{\partial \hat{\theta}}{\partial z} + K_{\theta l} \cos(\gamma). \quad (20)$$

3. NUMERICAL METHOD

3.1 Method of Lines (MoL).

The set of coupled partial differential equations (PDEs) are solved numerically using the Method of Lines (MoL) template developed by Lee et al (2004) using Matlab. In general, the MoL solves PDEs by discretising the spatial component of the PDE while keeping the time component continuous. For a coupled set of PDEs, the discretisation results in a system of ordinary differential equations (ODEs) of the form

$$d[\boldsymbol{\theta}, \mathbf{T}]/dt = \mathbf{f}([\boldsymbol{\theta}, \mathbf{T}], t) \tag{21}$$

where the bold represents a vector. For all test cases considered, Matlab's ODE15s was used to integrate (21). The spatial domain is discretised using a finite difference scheme developed by Schiesser (1991), which unlike conventional finite differencing schemes, does not incorporate boundary conditions directly into the finite difference equations. Instead, Schiesser's approach uses a series of upwinding and downwinding finite difference equations to account for the boundaries. Boundary conditions are incorporated by imposing the condition on an appropriate vector within the model depending on the type of boundary condition. A Dirichlet condition is imposed directly on the vector **θ** or **T** at the boundary node while Neumann conditions are imposed on the spatial gradient vectors $d\boldsymbol{\theta}/dz$ or $d\mathbf{T}/dz$ overwriting the finite differencing approximation at the boundary node (Schiesser, 1991; Lee et al, 2004).

Using this approach, incorporating boundary conditions given by (4)-(6) and (8)-(10) into the numerical method is straight forward except for the interface boundary condition ((5) and (9)). Following an approach by Matthews et al (2004), it is assumed that the finite differencing scheme can accurately approximate spatial gradients just above the interface for both solution variables θ and T. Therefore, the continuity of flux condition at the interface can be written in the general matrix form

$$\underbrace{\begin{bmatrix} -D_{T2} & -D_{\theta 2} \\ -\lambda - LD_{T2} & -LD_{\theta 2} \end{bmatrix}}_{\mathbf{A}} \begin{bmatrix} \partial T_2/\partial z \\ \partial \theta_2/\partial z \end{bmatrix} = \underbrace{\begin{bmatrix} q_{h1} \\ q_{\theta 1} - K_2 \cos(\gamma) \end{bmatrix}}_{\mathbf{b}}, \quad z = z_c, \tag{22}$$

where matrix **A** and **b** are known at each time interval. (22) is readily solved for $\partial T_2/\partial z$ and $\partial \theta_2/\partial z$, which is then used to construct an ODE at the interface in terms of Soil 2 for $\partial T_2/\partial t$ and $\partial \theta_2/\partial t$ thereby gaining a solution for T_2 and θ_2 at the interface. At the next time interval, T_1 and θ_1 are calculated from the new values of T_2 and θ_2 through the continuity of ψ and T conditions given in (5) and (9). Note that this approach has been shown to handle the discontinuity in θ at the interface between the two soils (Matthews et al, 2004).

3.2. Analytical solution for Divergence Length.

Warrick et al (1997) derived an analytical expression for divergence length under isothermal conditions, which is given by

$$\hat{L}_d = \hat{Q}_h / q_s , \tag{23}$$

$$\hat{Q}_h = -\tan(\gamma) \int_{\theta_{s1}}^{\theta_{1c}} D_1(\theta_1)\, \mathrm{d}\theta , \tag{24}$$

where $\hat{Q}_h$ is total horizontal flow (cm^2 sec^{-1}) along the x^*-axis (Figure 1), θ_{s1} and θ_{c1} is the water content at the surface and interface boundary in terms of Soil 1 and γ is the slope angle. For non-isothermal conditions, it can be shown that total horizontal flux can be expressed as

$$Q_h = -\tan(\gamma) \left[\int_0^{z_c} D_{\theta 1} \frac{\partial \theta_1}{\partial z} \mathrm{d}z + \int_0^{z_c} D_{T1} \frac{\partial T_1}{\partial z} \mathrm{d}z \right]. \tag{25}$$

Equations (23) and (25) will be used to approximate the divergence length under non-isothermal conditions by using the solution profile to numerical integrate (25) over the Soil 1 using Simpson's rule. Note that (25) has two components, i.e. the total horizontal flow due to a water gradient and total horizontal flow due to a temperature gradient. Consequently, we can calculate the contribution these gradients have to the divergence length via (23). Therefore, we will denote the divergence length due to a water gradient and a temperature gradient as L_d^θ and L_d^T, respectively. In addition, we will denote isothermal and non-isothermal divergence length by $\hat{L}_d$ and L_d, respectively. Note that $L_d = L_d^\theta + L_d^T$.

4. RESULTS AND DISCUSSION

This study will simulate coupled heat and water flow through a capillary barrier that consists of a Glendale clay loam over Berino fine sand. The hydraulic and thermal properties of the soil are given in Table 1. Note that, the additional soil parameters for the thermal properties are given by f_c for η and X_m and X_o for C_T and are only representative figures. Also, the isothermal hydraulic properties for both soils are described by van Genuchten (1980) equations with $m = 1 - 1/n$. For each test case considered, the soil profile was kept constant at a total length of $z_L = 70$ cm with the interface situated

at $z_c = 30$ cm and the initial water content in both layers was set at $\theta_{i1} = 0.248$ and $\theta_{i2} = 0.034$ corresponding to a constant matric potential of $\psi_i = -1000$ cm.

Table 1. Hydraulic and thermal properties for the Glendale clay loam and Berino fine sand.

Soil properties	clay loam	fine sand
θ_r	0.1060	0.0286
θ_s	0.4686	0.3658
α_{vg}	0.0104	0.0280
N	1.3954	2.2390
K_s	13.1	541.0
f_c	0.25	0.01
X_m	0.3	0.55
X_o	0.2314	0.0842

Also for the above test case, isothermal flow will be modeled using (19) and (20) under the same initial condition given by (3) and the same type of boundary conditions i.e. a constant surface flux and a free drainage condition. To highlight the effect of heat, the relative difference between the isotheral and non-isothermal case for each node within the system will be calculated as

$$RD_i = \frac{(\theta_i - \hat{\theta}_i)}{\theta_i}, \qquad (26)$$

where i is the node counter and ^ represents the isothermal solution.

4.1. Vertical Case.

The first test case considered was for a vertical soil profile ($\gamma = 0$ degrees) with a constant flux of $q_s = 1$ m year^{-1}. Figure 2 (a) and (b) show a plot of water content and temperature over depth of the soil profile at $t = 1, 3, 5, 7, 9$ and 10 days. Figure 2(a) clearly shows the effect of the constant flux infiltration at the surface of the soil profile and moisture transfer in the bottom soil layer due to temperature effects.

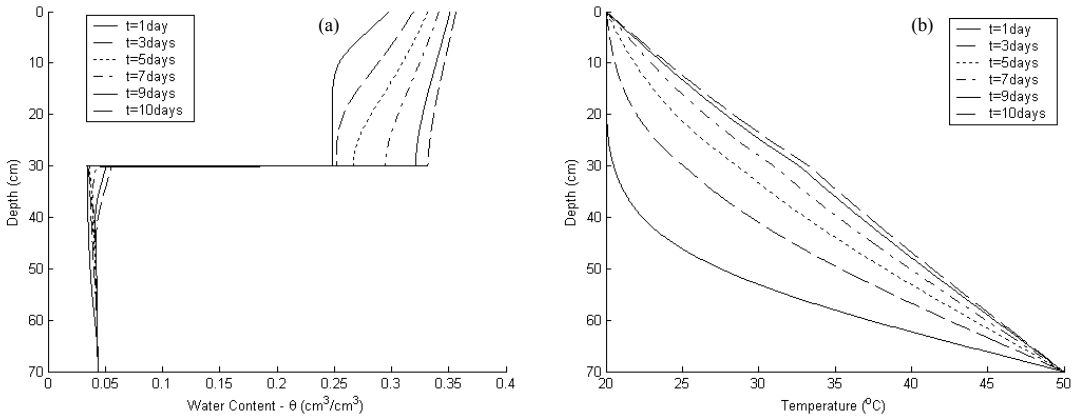

Figure 2 Plot of depth vs (a) water content and (b) temperature for $q_s = 1$ m year^{-1} at $t = 1, 3, 5, 7, 9$ and 10 days.

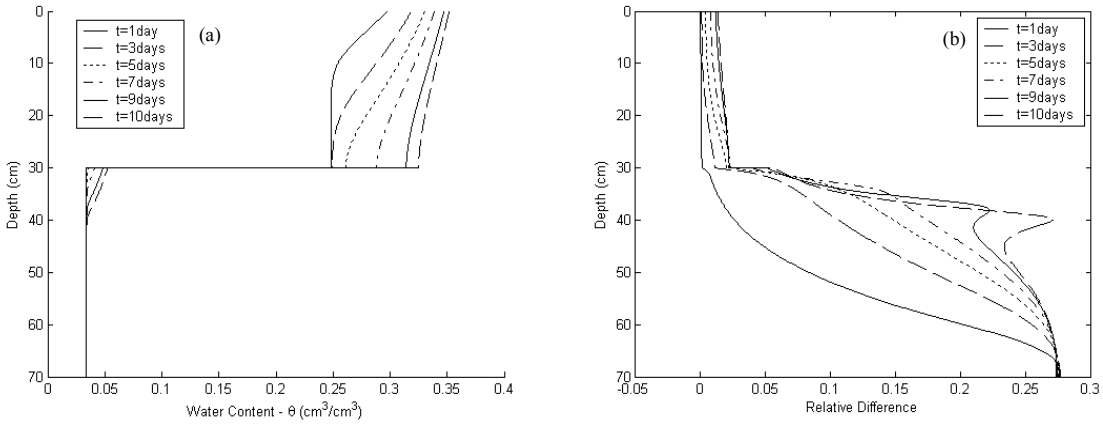

Figure 3. Plot of depth vs (a) water content for the isothermal case and (b) relative difference between the isothermal and non-isothermal cases for $q_s = 1$ m year^{-1} at $t = 1, 3, 5, 7, 9$ and 10 days.

In Figure 2(b), it is evident that the temperature distribution is moving towards an almost linear profile at t = 10 days. Also, the differences in the soil properties are only evident in the later simulation times at t = 9 and 10 days. At the later simulation times, heat transfer due to conduction is more prominent, which relies on the thermal properties of the soil matter and the water content (de Vries, 1958).

Figure 3(a) shows a plot of water content over depth of an isothermal solution for q_s = 1 m year^{-1} at t = 1, 3, 5, 7, 9, 10 days. From figure 3(a), it is evident that the bottom layer exhibits more thermal moisture movement as compared to the upper layer. On comparing figure 2(a) and 3(a), the bottom of the non-isothermal case is becoming wetter at the bottom of the soil profile. This is caused by the continual thermal transfer of water in the vapor phase from the infinite soil profile. Figure 3(b) shows a plot of relative difference between the isothermal and non-isothermal profiles calculated using (26). The increase in the θ in the bottom layer is evident and thermal transfer of water has also affected the top layer but to a lesser extent. Note that at approximately z = 40 cm the relative difference profiles at t = 9 and 10 days start to bulge demonstrating that a zone of higher water content is gather in the soil profile, which will then move downwards over time. This bulge is directly caused by the opposing water and heat fluxes where the water in the vapor phase is combining with the approaching wetting front from the constant infiltration. Given that we have opposing water fluxes due to infiltration and thermal transfer, it would be interesting to examine how this affects the divergence length for sloping profiles.

4.2. Effect on divergence capacity (L_d).

Table 2 shows the total divergence length of the capillary barrier under isothermal ($\hat{L}_d$) and non-isothermal conditions (L_d) for a range of constant surface fluxes and slope angles. For L_d, Table 2 also shows the contribution thermal gradients and water gradients have on L_d, which are represented by L_d^T and L_d^θ, respectively. Note that a positive divergence length denotes a downslope divergence while a negative divergence length denotes an upslope divergence. For cover liner design, downslope divergence is preferred to divert water away from the underlying waste.

Table 2 clearly shows the effect of the slope where all isothermal and non-isothermal divergence lengths increase as the slope increases for a given surface flux. This is to be expected since both (24) and (25) are multiplied by a factor of tan(γ) (Warrick et al, 1997). As the constant surface flux is increased, the isothermal divergence length ($\hat{L}_d$) moves from a downslope divergence at q_s = 0.01 and 0.1 m yr^{-1} to an upslope divergence at q_s= 1 m yr^{-1}. Interestingly, for non-isothermal flow, the opposite occurs where L_d shows an upslope divergence for the lower surface fluxes and a downslope divergence for the higher flux of 1 m yr^{-1}. On inspection of the two components of L_d, it is evident that L_d^T, for all values of q_s and γ considered, shows an upslope divergence that increases as the surface flux decreases. On the other hand, L_d^θ for all cases considered shows a downslope divergence, which also decreases as q_s increases. However, the decrease in L_d^θ is much more gradual than L_d^T, which eventually results in the positive values for L_d. The constant upslope divergence for L_d^T is caused by the thermal movement of water back up through the soil profile, i.e. from hotter to cooler regions (see Figure 3(b)), which is more predominant under drier conditions (de Vries, 1958).

Table 2. Horizontal Flux (Q_h) and divergence length (L_d) at varying angles and fluxes for the capillary barrier.

q_s (m y^{-1})	γ	L_d^θ (cm)	L_d^T (cm^{-1})	L_d (cm)	$\hat{L}_d$ (cm)
0.01	5	7.02x10^{0}	-1.91x10^{1}	-1.21x10^{1}	1.87x10^{1}
	10	1.43x10^{1}	-3.89x10^{1}	-2.46x10^{1}	3.73x10^{1}
	15	2.22x10^{1}	-6.03x10^{1}	-3.81x10^{1}	5.50x10^{1}
0.1	5	1.90x10^{0}	-1.91x10^{0}	-1.33x10^{-2}	4.19x10^{0}
	10	3.85x10^{0}	-3.89 x10^{0}	-4.70x10^{-2}	8.36x10^{0}
	15	5.91x10^{0}	-6.03x10^{0}	-1.27x10^{-1}	1.25x10^{1}
1	5	4.97x10^{-1}	-3.98x10^{-1}	9.90x10^{-2}	-3.25x10^{-1}
	10	1.69x10^{0}	-7.66x10^{-1}	9.32x10^{-1}	-6.42x10^{-1}
	15	2.69x10^{0}	-1.18x10^{-1}	1.51x10^{0}	-9.91x10^{-1}

As the surface flux increases, the downward movement of water increases, diminishing the effect of water fluxes due to thermal gradients. Even though it is not explicitly shown here, as q_s is increased further the above trend continues with L_d showing a downslope divergence as opposed to an upslope divergence for isothermal flow ($\hat{L}_d$). This result has implications for cover liner design since the divergence capacity of a capillary barrier can be increased, particularly under high surfaces fluxes, as long as the waste provides a source of heat. However, more work is required to gain a better understanding of the function of heat in promoting downslope divergence and its implications for cover liner design.

5. CONCLUSION

This paper has modeled coupled heat and water flow through a capillary barrier, which functions as a water barrier in a cover liner system. The results have shown that heat generated from the waste will have a dramatic effect on the functioning of the capillary barrier particularly in terms of its divergence length. Under dry conditions, the heat processes dominate resulting in upslope divergence, whereas for isothermal flow downslope divergence is expected under the same water flow conditions. Interestingly, as q_s is increased, the results show a downslope divergence under non-isothermal conditions when upslope divergence occurs in the isothermal case. This result has implications for cover liner design and highlights the need to gain a better understanding of non-isothermal flow through cover liner systems.

6. ACKNOWLEDGMENTS

This research has been funded under the ARC Discovery Indigenous Research Development program.

7. REFERENCES

Daniel, D.E. (1995), Soil barrier layers versus geosynthetic barriers in landfill cover systems, in *Landfill Closures: Environmental Protection and Land Recovery*, eds J. Dunn and U.P. Singh, American Society of Civil Engineers, New York.

de Vries, D.A. (1958), Simultaneous transfer of heat and moisture in porous media, *Transactions American Geophysical Union*, 39(5): 909-916.

Koerner, R.M., and D. E. Daniel. 1997. *Final Covers for Solid Waste Landfills and Abandoned Dumps*. 3rd ed., American Society of Civil Engineers (ASCE) Press, Virginia.

Lee, H.S., C.J. Matthews, R.D. Braddock, G.C. Sander, F. Gandola (2004), A MATLAB method of lines template for transport equations, *Environmental Modelling & Software*, 19: 603-614.

Matthews, C.J., R.D. Braddock and G.C. Sander (2004b), Modeling flow through a one-dimensional multi-layered soil profile using the Method of Lines, *Environmental Modeling and Assessment*, 9: 103-113.

Nassar, I.N., J.G. Benjamin and R. Horton (1996), Thermally induced water movment in uniform clayey soil, *Soil Science*, 161(8): 471-479.

Nassar, I.N. and R. Horton (1997), Heat, water, and solute transfer in unsaturated porous media: I – Theory development and transport coefficient evaluation, *Transport in Porous Media*, 27: 17-38.

Philip, J.R. and D.A. de Vries (1957), Moisture movement in porous media under temperature gradients, *Transactions American Geophysical Union*, 38: 222-232.

Scanlon, B.R., K. Keese and R.C. Reedy (2003), Variations in flow and transport in thick desert vadose zones in response to paleoclimatic forcing (0-90 kyr): Field measurements, modeling and uncertainties, *Water Resources Research*, 39(7): SBH3-1-SBH3-17.

Schiesser, W.E. (1991), *The Numerical Method of Lines: Integration of Partial Differential Equations*, Academic Press, Inc., San Diego.

van Genuchten, M.Th. (1980), A closed-form equation for predicting the hydraulic conductivity of unsaturated soils, *Soil Science of America Journal*, 44: 892-898.

Walter, M.T., J.-S. Kim, T.S. Steenhuis, J.-Y. Parlange, A. Heilig, R.D. Braddock, J.S. Selker and J. Boll (2000), Funneled flow mechanisms in a sloping layered soil: Laboratory investigation, *Water Resources Research*, 36(4): 841-849.

Warrick, A.W., P.J. Wierenga and L. Pan (1997), Downward water flow through sloping layers in the vadose zone: analytical solutions for diversions, *Journal of Hydrology*, 192: 321-337.